Geomicrobiology Journal, 26:606–622, 2009

ISSN: 0149-0451 print / 1521-0529 online
DOI: 10.1080/01490450903263392

Taylor & Francis
Taylor & Francis Group

Redox Speciation and Distribution within Diverse Iron-dominated Microbial Habitats at Loihi Seamount

Brian T. Glazer[1] and Olivier J. Rouxel[2]

[1]*Department of Oceanography, University of Hawaii, Honolulu, Hawaii, USA*
[2]*Woods Hole Oceanographic Institution, Marine Chemistry and Geochemistry Dept. Woods Hole, Massachusetts, USA*

Deep-sea hydrothermal systems such as the Loihi Seamount hydrothermal field are important examples of environments where both chemical and biological oxidation of Fe can occur simultaneously, and provide an ideal system to study the speciation and distribution of redox-sensitive bio-reactive elements such as Fe, Mn and S. A total of 13 discrete ROV dives were conducted within the Loihi Summit area over three cruises in 2006, 2007, and 2008. Here, we present and compare data from 17 distinct sites of historical and current interest, from focused and diffuse hydrothermal flow localities, over the three-year sampling period. We coupled an *in situ* electrochemical analyzer (ISEA) to a sensor wand and a high-resolution *in situ* micromanipulator deployed from ROV *Jason-II* to measure dissolved redox species within hydrothermal fluids and microbial mats at Loihi Seamount in complement to analyses on discrete samples collected using Titanium samplers. We compare *in situ* electrochemical data with traditional geochemical sampling and analysis techniques, and provide a geochemical context for past, on-going, and planned microbial ecology studies.

Keywords hydrothermal, iron, Loihi Seamount, microbial mats, suboxic, voltammetry.

Received 14 April 2009; accepted 3 August 2009.

None of this work would have been possible without the gracious invitation for collaboration from the Iron-Oxidizing Microbial Observatory Project (FeMO) Principle Investigators: Katrina Edwards (USC), Dave Emerson (Bigelow), Craig Moyer (WWU), Hubert Staudigel (UCSD-SIO), and Brad Tebo (OHSU). We thank them for their support and input during cruise operations, data analyses, and manuscript preparation. Two anonymous referees provided valuable comments on an earlier version of this manuscript. We thank the ROV *Jason-II* pilots and the crews of the RV *Melville*, RV *Kilo Moana*, and RV *T. Thompson* for assistance with deployments and sample collection during the cruises. We are grateful to Rebecca Briggs, In Chieh Chen, Jennifer Murphy, and Amanda Ricardo (UH) for assistance with electrochemical preparations, deployments, and *in situ* scan collections. We thank Maureen Auro (WHOI), Jessica Sharkey (MBARI) and Roman Barco (USC) for assistance with fluid sampling and analysis. We thank Geoff Wheat (UAF/MBARI) for Mg analyses. Thanks to Zensho Heshiki, Mike Cole (UH), and Donald Nuzzio (AIS, Inc.) for micromanipulator modifications and ISEA upgrades. We thank Wolfgang Bach (MPI) and Jan Amend (WUSTL) for bioenergetic discussions. This research was partially funded by the NSF Microbial Observatories program (KE, CM, DE, BT, HS) and a supplemental subcontract award to Glazer. The University of Hawaii NASA Astrobiology Institute, School of Ocean and Earth Science and Technology, and NSF-OCE 06-48637 also provided support for the *in situ* micromanipulator and deployable ISEA equipment. Support for Rouxel was provided by funding from the WHOI Deep Ocean Exploration Institute, Frank and Lisina Hoch Endowed Fund and NSF-OCE 0647948 and 0550066.

Address correspondence to Brian T. Glazer, Department of Oceanography, University of Hawaii, Marine Science Building 205, 1000 Pope Rd., Honolulu, HI 96822 USA. E-mail: glazer@hawaii.edu

INTRODUCTION

Seafloor hydrothermal activity is one of the fundamental processes controlling the exchange of heat and chemical species, including iron, between seawater and ocean rocks (Edmond et al. 1979; Elderfield and Schultz 1996; Stein and Stein 1994; Wheat et al. 2004). The abundance of Fe in high-temperature hydrothermal fluids at mid-ocean ridges and volcanic seamounts, along with its oxidation-reduction properties, confers it a particularly important role in both the chemistry and biology of near-field seafloor hydrothermal environments (e.g., Edwards et al. 2004). While the biogeochemical importance of iron has long been appreciated, only recently has evidence been building that recognizes the intense interdependence between microbes and iron speciation, as iron can serve as both an electron donor for lithotrophic growth and an electron acceptor for anaerobic respiration (e.g., Lovely 1991; Emerson and Moyer 1997).

Considerable prior efforts have focused on the geology, geochemistry, and microbiology of Loihi Seamount (e.g., Moyer et al. 1994; Garcia et al. 2006; Malahof et al. 2006). Loihi is the youngest volcano in the Hawaiian Chain, rising ∼4 km above the abyssal plain to a depth about 960m below sea surface (Figure 1). Hydrothermal venting is best described near the summit, and studies on the microbiology of Loihi have closely mirrored those on the chemical evolution of hydrothermal fluids (e.g., Karl et al. 1988; Sedwick et al. 1992; Moyer et al. 1994, 1995, 1998; Wheat et al. 2000; Emerson and Moyer 2002).

Vent fluids at Loihi are typically highly enriched in CO_2, CH_4, NH_4, PO_4, Fe, and Mn (Karl et al. 1988; Sedwick et al. 1992; Wheat et al. 2000) and depleted in H_2S, rendering Loihi

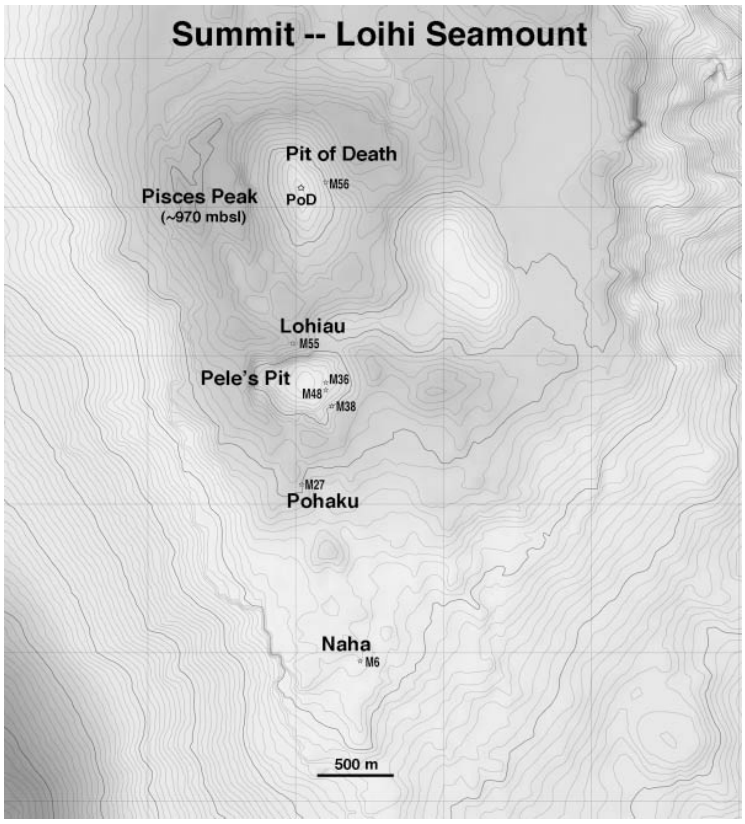

FIG. 1. Bathymetric contour map (100m intervals) with shaded relief of Loihi Seamount showing location of important sampling sites (Courtesy Anthony Koppers, SIO). In general, sampling sites can be described by general area: Spillway Area (Mkr 34 & 38), Hiolo Area (Mkr 36 & 39), Tower Area (Mkr 31 & 48, north of Mkr 38), Lohiau Area (Mkr 2, 5, 55), Pohaku Area (Mkr 27 & 57), Naha Area (Mkr 1, 3, 6), and Pit of Death Area (Mkr 56).

distinct from mid-ocean ridge hydrothermal systems. Loihi vent fields support abundant and diverse prokaryotic populations, particularly among the Fe-oxidizing bacteria (FeOB). A variety of filamentous, non-filamentous, tubular, and branching FeOB are recognized in massive microbial mats (Karl et al. 1988; Emerson and Moyer 2002). Previous studies combining terminal-restriction fragment length polymorphism (T-RFLP), culturing studies, and FeOB morphology demonstrated that lithotrophic FeOB are abundant and active at Loihi, and that biological Fe-oxidation contributes up to ∼60% of total Fe-oxidation (Emerson and Moyer 2002).

Hence, Loihi Seamount presents ideal opportunities to study the impact of redox speciation and distribution within diverse iron-dominated microbial habitats, because of slowed abiotic Fe oxidation, due to the unique conjunction of chemical composition of the hydrothermal fluids with high Fe and CO_2 concentrations, resulting in lower pH conditions (5.3–5.5), and low O_2 concentration in ambient seawater at ∼1,000 m depth (O_2 ∼50 μM) associated with the oxygen minimum zone (OMZ).

Here, we report on the systematic surveying and sampling of the Loihi Summit pit crater system over a period of three ROV *Jason-II* cruises (2006–2008). We report specific details regarding the temporal and spatial variability in the physical and geochemical settings, particularly within the context of iron-oxidizing bacteria (FeOB) habitat. Using an *in situ* electrochemical analyzer, we have explored a range of environmental niches where the kinetics of abiotic oxidation are sluggish, and biologically favorable conditions prevail, allowing microbes to be competitive with abiotic reactions. Diversity, distribution, and function of the associated microbial communities are reported elsewhere in this issue.

SAMPLING AND ANALYTICAL METHODS

Through close collaboration with a NSF-funded Microbial Observatory Program conducted at Loihi Seamount (Iron-Oxidizing Microbial Observatory, FeMO; led by Edwards, Moyer, Emerson, Tebo, Staudigel), we participated in three cruises onboard R/V *Melville* (October 2006), RV *Kilo Moana* (2007) and RV *T. Thompson* (2008). During these cruises, we conducted a suite of *in situ* temperature and voltammetric analyses and discrete hydrothermal fluid sampling using ROV *Jason-II* as described later.

TABLE 1
Selected electrode reactions at the Au/Hg electrode vs. the Ag/AgCl reference electrode. All data were obtained with a 100 μm diameter electrode. (MDL – Minimum Detection Limit, adapted from Luther et al. 2008).

	E_p ($E_{1/2}$) (V)	MDL (μM)
$O_2 + 2H^+ + 2e^- \rightarrow H_2O_2$	−0.33	3
$HS^- + Hg \rightarrow HgS + H^+ + 2e^-$	Adsorption onto Hg	<−0.60
$HgS + H^+ + 2e^- \leftrightarrow HS^- + Hg$	∼−0.60	<0.1
$S^0 + Hg \rightarrow HgS$	Adsorption onto Hg	<−0.60
$HgS + H^+ + 2e^- \leftrightarrow HS^- + Hg$	∼−0.60	<0.1
$Hg + S_x^{2-} \leftrightarrow HgS_x + 2e^-$	Adsorption onto Hg	<−0.60
$HgS_x + 2e^- \leftrightarrow Hg + S_x^{2-}$	∼−0.60	<0.1
$S_x^{2-} + xH^+ + (2x\text{-}2)e^- \leftrightarrow xHS^-$	∼−0.60	<0.1
$2\,RSH \leftrightarrow Hg(SR)_2 + 2H^+ + 2e^-$	typically more positive than H_2S/HS^-	
$2\,S_2O_3^{2-} + Hg \leftrightarrow Hg(S_2O_3)_2^{2-} + 2e^-$	−0.15	10
$S_4O_6^{2-} + 2e^- \rightarrow 2\,S_2O_3^{2-}$	−0.45	15
$FeS + 2e^- + H^+ \rightarrow Fe(Hg) + HS^-$	−1.15	molecular species
$Fe^{2+} + Hg + 2e^- \leftrightarrow Fe(Hg)$	−1.43	10
$Fe^{3+} + e^- \leftrightarrow Fe^{2+}$	−0.2 to −0.9	molecular species
$Mn^{2+} + Hg + 2e^- \leftrightarrow Mn(Hg)$	−1.55	5
$Zn^{2+} + Hg + 2e^- \leftrightarrow Zn(Hg)$	−1.02	<0.1

Temperature and In Situ Analyses

Important progress has been made in recent years using *in situ* voltammetric techniques for geochemical characterization of coastal bottom waters and sediments (e.g., Luther et al. 1999; Lewis et al. 2007; Taillefert et al. 2007), water column oxic-anoxic transitions (e.g., Konovalov et al. 2003; Glazer et al. 2006a, 2006b), microbial mats (e.g., Luther et al. 2001; Glazer et al. 2002), and hydrothermal vents (e.g., Luther et al. 2001; Hsu-Kim et al. 2008). A key benefit to using voltammetry is the capability for collecting simultaneous measurements of dissolved O_2, H_2S, Mn^{2+}, Fe^{2+}, $S_2O_3^{2-}$, $S_4O_6^{2-}$, S_x^{2-}, soluble S^0 and aqueous species of FeS and organic Fe^{3+}, if present at detectable concentrations (e.g., Luther et al. 2008 for recent review; Table 1). We interfaced an *in situ* electrochemical analyzer, ISEA, (ISEA-III, Analytical Instrument Systems, Inc., Flemington, NJ, USA) to the ROV *Jason-II* in a manner similar to previously-described successful deployments (e.g., Luther et al. 2008). Briefly, four voltammetric microelectrodes were deployed in one of two ways for geochemical redox surveying of hydrothermal fluids and microbial mats: (i) mated to the ROV temperature wand for widespread surveying and "macro-profiling" (∼1 cm minimum vertical travel increments, Figure 2A), or (ii) mounted on an *in situ* micromanipulator (AIS, Inc.) for high-resolution profiling across the sediment-water interface (0.1 mm minimum vertical travel increments, Figure 2F).

We custom-designed a compact, versatile tripod to house the micromanipulator and allow efficient transport, deployment, and recovery by the ROV (micro-adjustable non-intrusive profiler, MANIP; Figure 2F; Glazer et al., unpublished). The custom solid-state Au/Hg working electrodes, Ag/AgCl reference electrodes, and Pt counter electrodes were constructed from durable 3mm diameter PEEK tubing and epoxy using previously described methods, and calibrated using standard electrochemical calibration methods (e.g., Brendel and Luther 1995; Glazer et al. 2004; Luther et al. 2008). When not in use, the wand and MANIP were stowed in custom holsters and brackets mounted on the science basket of the ROV *Jason-II*. An electrochemistry operator in the ROV control van communicated with the ISEA (and MANIP) using a laptop interfaced with the ROV fiber optic cable. Parameters for individual voltammetric scans were typically set as follows: initial conditioning steps of −0.9 V for 5s and −0.1 V for 2 s, then performing cyclic voltammetry by scanning from −0.1 V to −1.85 V and back to −0.1 V at a scan rate of 500–2000 mV s^{-1}. Square wave voltammetry was also typically performed in areas of low flow and turbulence (scan rate of 250 mVs^{-1}). Temperature and voltammetric scans were simultaneously visualized in real time, and current peaks (or absence thereof) were immediately identified for qualitative characterization of detectable chemical redox species for each given sampling site. On-the-fly concentration estimates could be provided based upon comparisons to electrode calibrations made prior to deployments, allowing for high-quality site selection for discrete sample collection and deployment of microbial colonization experiments. All electrochemical data were saved to computer disk and rigorously analyzed and compared with calibration datasets following the cruises. Individual scan analysis took place using a combination of the manufacturer's software (Advanced Analysis, AIS, Inc.), open-source voltammetric analysis software (*Voltint*, Bristow and Taillefert 2008), and a custom auto-analysis package being developed at UH (Glazer, unpublished).

Hydrothermal Fluid Sampling and Analysis

The real-time temperature and voltammetry measurements collected just prior to discrete sampling helped to optimize targeted sample location and increase likelihood for collection of fluids from orifices and chimneys producing the most reduced fluids in a localized sampling site that would be the most indicative of hydrothermal end-member composition. Hydrothermal fluid samples were collected using 750 ml titanium samplers (*Ti-samplers*) on-board ROV *Jason-II* (Figure 2B–2E). The operation of the Ti-samplers has been described previously (von Damm et al. 1985). Briefly, the Ti-samplers are filled using a titanium snorkel that can be inserted directly into the vent orifice. Verification of warm fluids entering the snorkel is made by visual indication of flow through an indicator weep-hole anterior to the sample chamber. Sample chambers are then filled by ROV triggering of a spring-loaded piston mechanism.

Immediately upon sample recovery, pH and alkalinity were measured. For all samples, an acidified and filtered (0.2 μm) sample split was subsequently archived for shore-based chemical analysis. The insoluble particles remaining in the Ti-samplers were recovered for chemical analysis when the samplers were disassembled by rinsing with Milli-Q water and

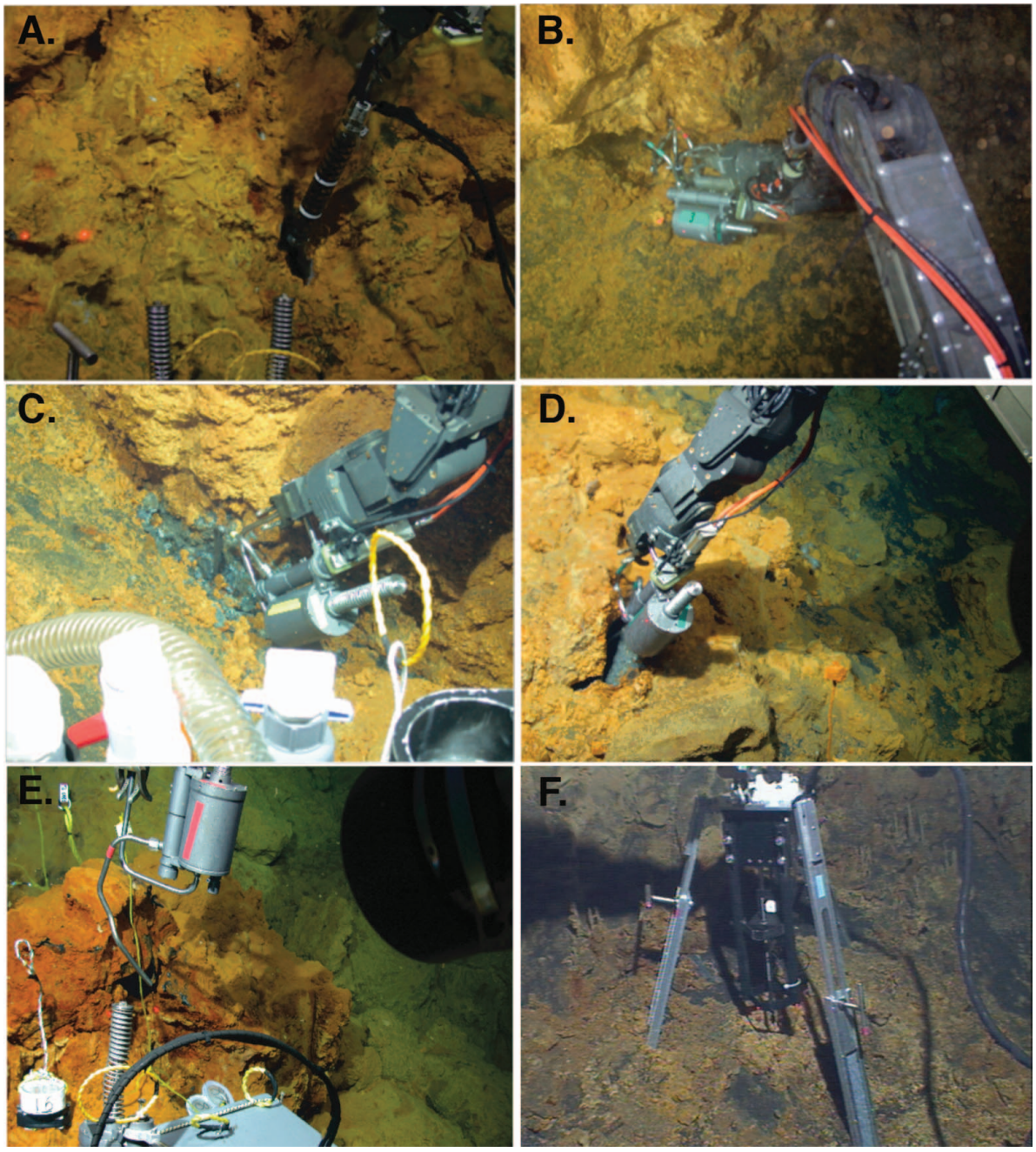

FIG. 2. Color photo of hydrothermal fluid surveying and sampling: (A) ROV *Jason-II* temperature probe combined with voltammetric electrode wand, J2-368, Mkr 39 (B) Titanium sampler positioned at orifice near Mkr 34, sample J2-241-10-MS3&4, (C) Titanium sampler positioned at orifice near Mkr 36, J2-365-MS-Yellow, (D) Titanium sampler positioned at orifice near Mkr 39, J2-365-MS-Green, (E) Titanium sampler positioned at orifice near Mkr 57, J2-368-MS-Red, (F) voltammetric microprofiling of microbial floc near Mkr 36.

acetone and filtered through 0.45 mm filters. This fraction, however, is not included in the final fluid analysis as it contains microbial mat debris entrained during sampling rather than particulate formed inside the Ti-sampler.

Fluid composition was determined by high-resolution ICPMS *Element2* operated at WHOI. Briefly, sample solutions, diluted to 1:7 with 2% HNO_3 (Optima grade), were analyzed using the high-resolution mode of the ICPMS which permits separation of isotopes from isobaric interferences, such as $^{40}Ar^{16}O^{1}H$ on ^{57}Fe. Indium solution was added to a final concentration of 5 ppb to correct for ICP MS sensitivity changes due to matrix effects. Solutions were introduced into the plasma using

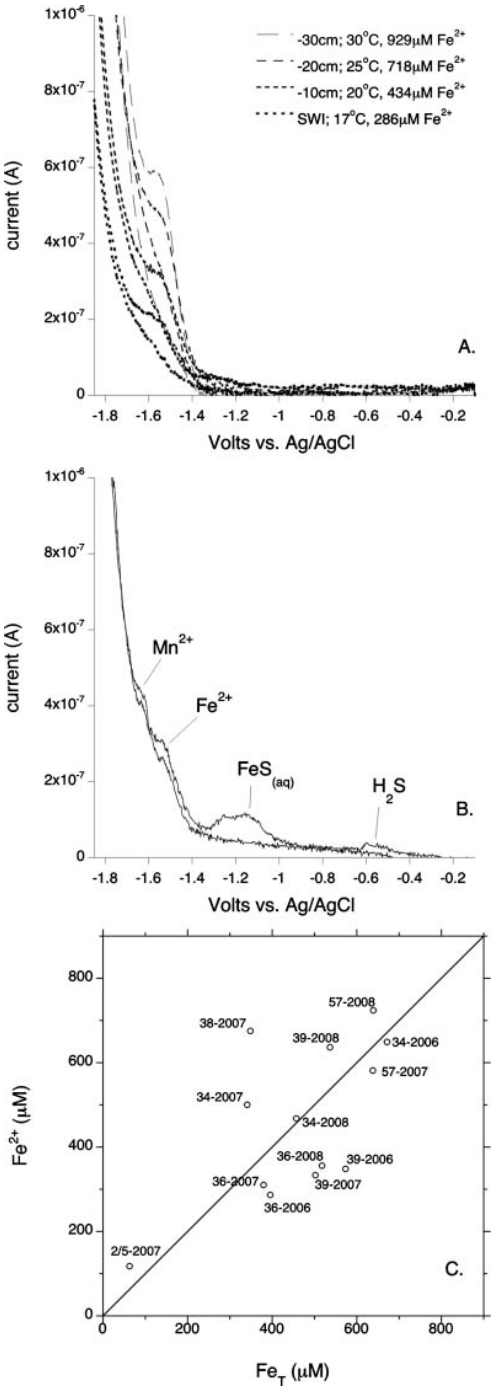

FIG. 3. Representative voltammograms collected during wand surveying of: (A) Pohaku flange macro profile, J2-316, Mkr 57; and (B) Hiolo vent orifice, J2-242, Mkr 39. At Pohaku, only Fe^{2+} was detectable, and increased with depth as the wand was penetrated into the diffuse flow. Conversely, in the venting orifice at Hiolo, multiple redox chemical species were present at detectable levels: Fe^{2+} = 421 μM, Mn^{2+} = 42 μM, H_2S = 4 μM, and $FeS_{(aq)}$ molecular clusters. (C) Direct comparison between in situ electrochemical iron measurements (dissolved Fe^{2+}) and total dissolved iron measurements from discrete measurements were generally in good agreement, with some deviation. See text for explanation.

a quartz spray chamber system equipped with a microconcentric PFA nebulizer operating at a flow rate of about 100 μL/min. For each element, ICPMS sensitivity was calibrated using matrix matched standard solutions corresponding to seawater matrices.

RESULTS

Surface ship and ROV surveying and sampling at Loihi took place in 2006 (RV *Melville*), 2007 (RV *Kilo Moana*) and 2008 (RV *Thomas Thompson*), and utilized ROV *Jason-II* in each year. A total of 13 ROV dives were conducted in the Loihi Summit area. A great advantage of ROV work at Loihi is that most of the sites are within a workable radius (Figure 1), allowing for multiple sites to be visited on a given lowering, and extending productive bottom time to up to 4 days per dive. Efficiency was often further enhanced by the use of free vehicle elevators to shuttle samplers and samples between the ROV and ship. Widespread temperature and electrochemical surveying was conducted at 17 discrete hydrothermal sites at the Loihi Summit. Generally, the capability for real-time fluid speciation information derived through voltammetric surveying was instrumental for efficiently collecting discrete samples for bulk fluid composition, as well as for identifying optimal locations for deployment of microbial colonization deployments (Figures 2 and 3). Among the Loihi Summit sites visited, we identified three important, distinct iron-dominated microbial habitats, with fluid composition driven by: (i) hydrothermal fluid endmember, (ii) turbulent mixing of hydrothermal endmember component with low-oxygen seawater endmember, and (iii) microbially-mediated diffuse flow flocs intermediate to (i) & (ii).

Hydrothermal Fluids

In this section, we present and compare data from multiple sites of historical and current interest, from focused and diffuse hydrothermal flow localities, over the three-year sampling history. We compare *in situ* electrochemical data with traditional geochemical sampling and analysis techniques (Figure 3C), and provide a geochemical context for past, ongoing, and planned microbial ecology studies. In general, vent fluids ranged in maximum temperature from 21.6°C to 55°C for actively discharging sites inside Pele's Pit and southern vents at Pohaku, whereas the Pit of Death site yielded temperature of 3.4°C above Fe-rich sediments and a maximum of 6°C within an iron floc, as compared with ambient seawater temperatures of 2.6°C. "Major" Ti-samplers were deployed only at Pele's Pit vents (Mkr5, Mkr34, Mkr38, Mkr36 and Mkr39) and Pohaku (Mkr57). A summary of the discrete samples recovered between 2006–2008 is presented in Table 2 together with sample location and description, vent temperature, pH, and chemical composition. Reported temperature for each fluid sample represents the maximum observed temperature from the vent orifice prior to, or after sampling. Chemical data are plotted against dissolved Si concentration (Figure 4), which is used to measure the extent of dilution of the hydrothermal fluid with background seawater (Sedwick et al., 1992 and Wheat et al., 2000). The use of Si

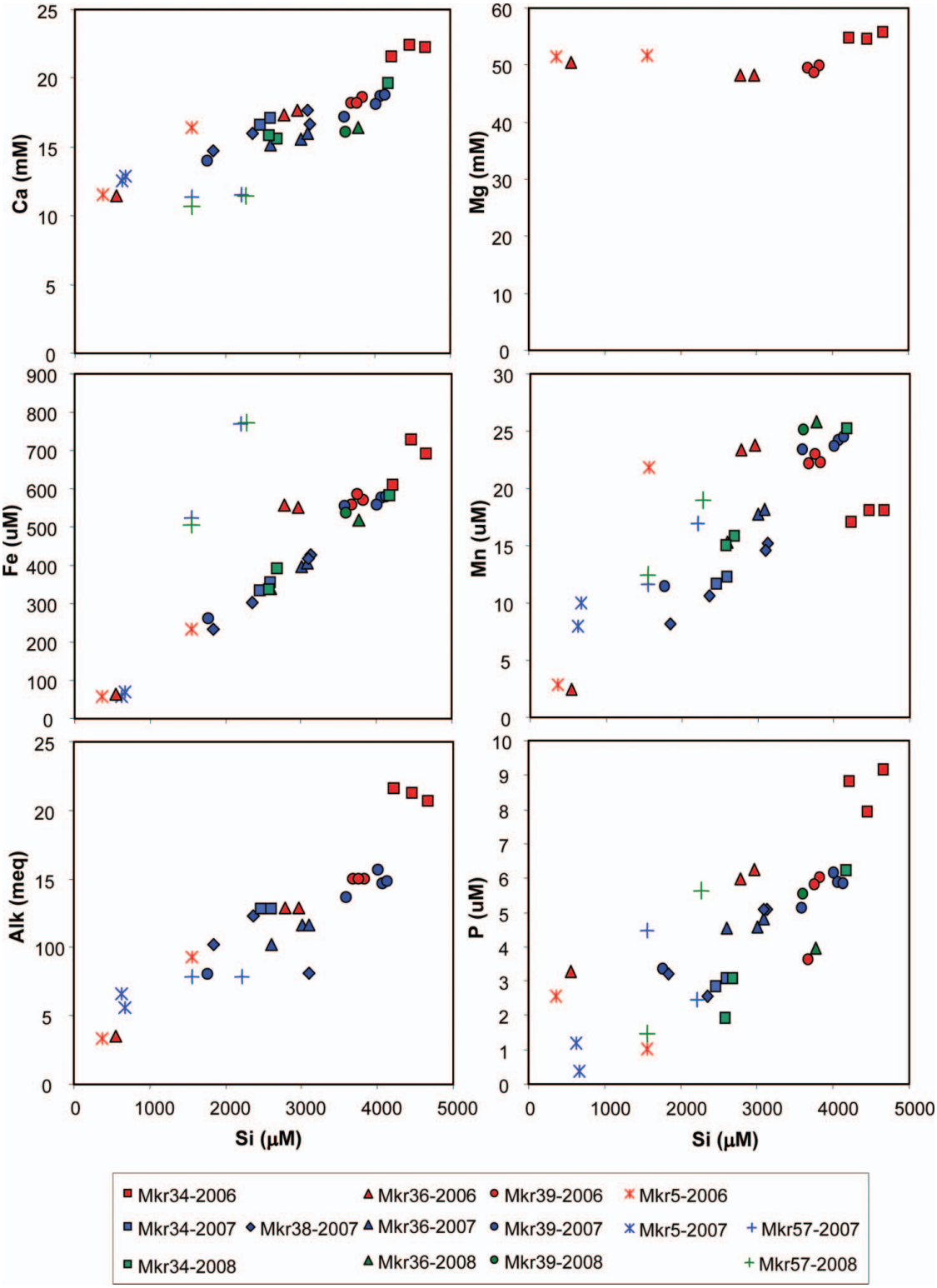

FIG. 4. Plots of concentrations of dissolved chemical species (Ca, Mg, Fe, Mn, alkalinity, P) versus Si for samples from Spillway Area (Mkr 34 & Mkr 38), Hiolo Area (Mkr 36 & Mkr 39), Lohiau Area (Mkr 2 & Mkr 5), and Pohaku Area Mkr 57).

TABLE 2
Chemical composition of discrete hydrothermal fluids at Loihi

Sample Name	Mkr#	Year	Temp C	pH	Alk meq/kg	Si μM	Mg mM	Ca mM	P μM	Fe μM	Mn μM	Fe/Mn
Spillway Area (Mkr 34 & 38)												
J2-365-MS-red	Mkr 34	2008	21.6	5.99		2691		15.6	3.1	391.4	15.8	24.8
J2-373-MS-black	Mkr 34	2008	51.5	5.83		2589		15.8	1.9	335.6	15.0	22.3
J2-373-MS-red	Mkr 34	2008	51.5	6.00		4180		19.6	6.2	580.4	25.2	23.0
J2-308-MS3-RL	Mkr 34	2007	47.0	6.72	12.8	2599		17.1	3.1	354.7	12.3	28.9
J2-308-MS4-RR	Mkr 34	2007	47.0	6.54	12.8	2464		16.6	2.8	333.2	11.6	28.7
J2-241-MS3	Mkr 34	2006	54.0	6.37	20.6	4664	55.8	22.2	9.1	690.2	18.1	38.2
J2-241-MS4	Mkr 34	2006	54.0	6.02	21.2	4464	54.5	22.4	7.9	726.7	18.1	40.1
J2-245-MS4	Mkr 34	2006	52.0	6.00	21.6	4226	54.7	21.6	8.8	609.9	17.0	35.9
J2-315-MS-RR	Mkr 38	2007	47.0			3129		16.6	5.1	426.6	15.2	28.1
J2-314-MS-RL	Mkr 38	2007	55.0	6.21	12.3	2360		16.0	2.6	303.9	10.6	28.6
J2-314-MS-RR	Mkr 38	2007	55.0	6.10	10.2	1840		14.7	3.2	234.2	8.1	28.8
J2-315-MS-RL	Mkr 38	2007	47.0	6.96	8.1	3096		17.7	5.1	419.0	14.5	28.8
Hiolo area (Mkr 36 & 39)												
J2-365-MS-yellow	Mkr 36	2008	44.0	5.75		3774		16.4	3.9	518.8	25.8	20.1
J2-314-MS-BL	Mkr 36	2007	50.0	6.29	10.2	2604		15.1	4.6	338.1	15.3	22.1
J2-314-MS-BR	Mkr 36	2007	50.0	5.84	11.7	3006		15.6	4.6	397.6	17.8	22.4
J2-315-MS-BR	Mkr 36	2007	51.0	6.02	11.6	3092		16.0	4.8	407.1	18.2	22.3
J2-241-MS1	Mkr 36	2006	51.0	6.01	12.9	2782	48.3	17.4	6.0	557.8	23.4	23.9
J2-241-MS2	Mkr 36	2006	51.0	6.00	3.5	551	50.5	11.5	3.3	64.0	2.5	25.8
J2-242-MS2	Mkr 36	2006	51.0	5.76	12.9	2966	48.2	17.6	6.2	552.3	23.8	23.2
J2-365-MS-green	Mkr 39	2008	43.2	5.82		3609		16.0	5.5	537.9	25.1	21.5
J2-308-MS1-BL	Mkr 39	2007	45.0	6.67	14.7	4069		18.7	5.9	576.0	24.1	23.9
J2-308-MS2-BR	Mkr 39	2007	45.0	6.69	14.8	4131		18.7	5.8	577.8	24.5	23.6
J2-311-MS-BL	Mkr 39	2007	47.4	6.29	8.1	1772		13.9	3.3	261.4	11.5	22.8
J2-311-MS-BR	Mkr 39	2007	47.4	6.21	13.7	3591		17.2	5.1	553.7	23.4	23.7
J2-315-MS-BL	Mkr 39	2007	52.0	6.08	15.6	4010		18.1	6.1	556.4	23.7	23.5
J2-242-MS3	Mkr 39	2006	51.0	5.88	15.0	3830	50.0	18.6	6.0	568.8	22.2	25.6
J2-242-MS4	Mkr 39	2006	51.0	5.94	15.0	3679	49.4	18.2	3.6	558.6	22.1	25.3
J2-245-MS2	Mkr 39	2006	50.0	5.77	15.0	3757	48.7	18.2	5.8	584.1	23.0	25.4
Lohiau Area (Mkr 2 &5)												
J2-311-MS-RL	Mkr 5	2007	24.5	6.94	5.6	675		12.9	0.4	68.3	10.0	6.8
J2-311-MS-RR	Mkr 5	2007	24.5	6.65	6.6	628		12.6	1.2	58.0	8.0	7.2
J2-242-MS1	Mkr 5	2006	21.0	6.21	3.4	369	51.5	11.5	2.5	57.7	2.8	20.4
J2-245-MS1	Mkr 5	2006	22.0	5.89	9.3	1558	51.8	16.5	1.0	234.7	21.8	10.8
Pohaku area (Mkr 57)												
J2-368-MS-black	Mkr 57	2008	28.3	6.52		1553		10.7	1.5	507.2	12.4	40.9
J2-368-MS-red	Mkr 57	2008	26.7	5.59		2275		11.4	5.6	773.4	19.0	40.7
J2-316-MS-RL	Mkr 57	2007	26.5	7.32	7.8	1556		11.3	4.5	524.2	11.7	44.9
J2-316-MS-RR	Mkr 57	2007	26.5	7.32	7.8	2210		11.6	2.4	769.4	16.9	45.5

instead of Mg is motivated by the fact that: (1) Mg concentrations remain very close to background seawater in contrast to most seafloor hydrothermal vents (Von Damm et al.), (2) Si concentrations in hydrothermal fluids are more than 20 times enriched relative to seawater, (3) Si behaves conservatively during mixing with seawater. *In situ* electrochemical measurements taken concurrently to temperature were made at all discrete sampling locations plus other sites, and are also detailed below (Table 3).

Spillway Area (Mkr34, Mkr38)

Marker 34 (Mkr34) (18.90537917N 155.25674311W 1271.954 m) is located along the scarp of the SE summit pit crater rim (Figure 1, Figure 2B). In 2006, 2007, and 2008,

TABLE 3
Loihi Summit Sites In Situ Electrochemistry mean concentrations reported; sd = standard deviation of the mean; n typically 5–10 per depth; nd = not detected

Dive #	Mkr#	Year	Wand Height (cm)	Temp (°C)	sd	O_2 (μM)	sd	Fe^{2+} (μM)	sd	Mn^{2+} (μM)	sd	HS^- (μM)	sd	Fe^{3+} (nA)	FeS_{aq} (nA)
Spillway Area (Mkr 34 & 38)															
365	Mkr34	2008	0	20.4		nd		467	15.5	nd		nd		nd	84.3
308	Mkr34	2007	0	50.0		nd		346	11.6	17		nd		nd	
314	Mkr34	2007	0	53.0		nd		555	64.1	9	2.1	3.36	1.5	nd	15
241	Mkr34	2006	0	52.0		nd		648	38.7	nd		nd		nd	nd
365	Mkr38	2008	0	25.7	0.25	nd		273	107	nd		34.0	4.2	nd	nd
314	Mkr38	2007	0	54.5		nd		695	31.4	nd		4.2	1.2	nd	nd
			−15	54.5		nd		775	30	nd		3.06	1	nd	nd
315	Mkr38	2007	0	47.0		nd		545	32	nd		nd		nd	nd
245	Mkr38	2006	0	24.0		nd		50	11.8	nd		nd		nd	nd
Hiolo Area (Mkr 36, 39, BT37, Finger Chimney)															
365	Mkr36	2008	0	44		nd		355	153	nd		6.1	8.4	nd	49.3
314	Mkr36	2007	0	46.0		nd		565	47.1	nd		23.8	2.5	nd	nd
315	Mkr36	2007	0	51.0		nd		117	8.18	18		17.15	3.3	nd	96.1
241	Mkr36	2006	2	10.1		nd		161	50.6	19	4.2	3.44	0.5	nd	nd
			0	24.9		nd		118	49.6	24	20	2.34	1.8	nd	5.7
			−2	45.0		nd		435	57.3	nd		nd		nd	12
			−4	48.0		nd		437	5.3	nd		nd		nd	nd
365	Mkr39	2008	−5	45		nd		636	33.8	nd		4.8	2.9	nd	37.4
308	Mkr39	2007	0	51.1	1.55	nd		212	26.6	18	4.8	15.86	3	nd	113
311	Mkr39	2007	0	49.5		nd		312	265	nd		56	15	nd	243
			−10	49.5		nd		799	93.8	nd		46.75	8.2	nd	318
315	Mkr39	2007	5	44.0		nd		126	134	26	3.3	24.36	7.3	nd	153
			0	52.0		nd		277	58.4	60		17.12	7.4	nd	111
242	Mkr39	2006	0	51.0		nd		347	42.7	33	19	4.2	0.5	nd	69
245	Mkr39	2006	0	50.7		nd		569	52.9	nd		nd		nd	nd
242	BT37	2006	0	11.0		nd		93	10.5	nd		nd		nd	nd
			−10	14.6		nd		224	37.6	nd		nd		nd	nd
242	FingChim	2006	0	21.0		nd		133	8.65	nd		nd		66.3	nd
			−1	21.0		nd		225	19.8	nd		nd		62	nd
			−17	20.8		nd		249	3.6	nd		nd		56.8	nd
Tower Area (Mkr 31 & 48)															
365	Mkr31	2008	−2	7.5		nd		108	36.1	nd		nd		nd	nd
308	Mkr31	2007	10	4.0		63	1.7	7	8.13	nd		nd		7.6	nd
			5	4.0		65	4.7	25	8.36	nd		nd		6.3	nd
			0	4.5		52	6.7	53	9.24	nd		nd		7.2	nd
			−10	13.0		nd		383	30.8	nd		nd		6.3	nd
311	Mkr31	2007	0	4.5		nd		150	4.7	nd		nd		nd	nd
			−5	9.0		nd		300	24.8	nd		nd		nd	nd
			−10	14.0		nd		324	5.58	nd		nd		nd	nd
			−20	25.0		nd		379		nd		nd		nd	nd
314	Mkr31	2007	0	8.0		nd		165	13.7	nd		nd		40	nd
			−15	12.0		nd		253	32	nd		nd		nd	nd
			−22	20.5		nd		347	10.3	nd		nd		nd	nd
315	Mkr31	2007	5	7.5		17	1.3	nd		nd		nd		nd	nd
			0	9.5		nd		109	11.6	nd		nd		nd	nd
			−5	11.0		nd		183	6.7	nd		nd		nd	nd

(Continued on next page)

TABLE 3
Loihi Summit Sites In Situ Electrochemistry mean concentrations reported; sd = standard deviation of the mean; n typically 5–10 per depth; nd = not detected *(Continued)*

Dive #	Mkr#	Year	Wand Height (cm)	Temp (°C)	sd	O_2 (μM)	sd	Fe^{2+} (μM)	sd	Mn^{2+} (μM)	sd	HS^- (μM)	sd	Fe^{3+} (nA)	FeS_{aq} (nA)
	−10	13.5		nd		178	5.9	nd		nd		nd	nd		
			−15	17.0		nd		284	50.1	nd		nd		nd	nd
			−25	28.0		nd		358	77.3	17	2.6	4.9	0.4	nd	nd
241	Mkr31	2006	5	9.4	0.28	29	5.9	nd		nd		nd		nd	nd
			0	9.2		23	12	nd		nd		nd		nd	nd
			−5	10.3		nd		448	6.34	nd		1.2	0.2	nd	nd
			−7	14.2	1.42	nd		449	10.9	nd		2.7	0.7	nd	nd
245	Mkr31	2006	0	3.2		nd		nd		nd		nd		nd	nd
			−4	20.6		nd		142	93.5	nd		nd		nd	nd
			−11	23.6		nd		411	28.8	nd		nd		nd	nd
315	Mkr48	2007	0	5.5		11	7.7	nd		nd		nd		nd	nd
			−5	11.0		nd	15	10		nd		nd		nd	nd
316	Mkr48	2007	5	5.0		33	5.8	nd		nd		nd		nd	nd
			−2	7.0		29	1.8	nd		nd		nd		nd	nd
			−10	12.0		9		nd		nd		nd		nd	nd
Lohiau Area (Mkr 2, 5, 55)															
308	Mkr2	2007	0	5.5		nd		138		nd		nd		nd	nd
			−5	9.5		nd		205	15.2	nd		nd		nd	nd
			−10	18.5		nd		226	6.26	nd		nd		nd	nd
			−412	19.0		nd		236	6.4	nd		nd		nd	nd
310	Mkr5	2007	5	4.5		35	1.4	nd		nd		nd		nd	nd
			−5	6.5		27	4.8	nd		nd		nd		nd	nd
			−15	8.5		13	2.5	11	0.6	nd		nd		nd	nd
			−20	9.5		nd		16	1.04	nd		nd		nd	nd
			−30	12.5		nd		94	5.2	nd		nd		nd	nd
Pohaku Area (Mkr 27 & 57)															
368	Mkr57	2008	0	21		nd		665		nd		nd		nd	nd
			−4	24		nd		723	58.7	nd		nd		nd	nd
			−10	24.3		nd		743	61.2	nd		nd		nd	nd
315	Mkr57	2007	0	17.3	2.05	8	2.1	300	49.3	nd		nd		5.4	nd
316	Mkr57	2007	0	17.5		nd		288	86.5	nd		nd		nd	nd
			−10	26.0		nd		812	162	nd		nd		nd	nd
			−30	30.0		nd		934	9.3	nd		nd		nd	nd
316	Mkr57	2007	0	20.0		nd		514	60.8	nd		nd		nd	nd

active venting was observed along the footwall and cracks, with very little Fe-rich flocs visible in the discharging cracks. Thin Fe-rich microbial mats line the vertical walls bathed in the rising shimmering fluids. Away from the scarp are volcanic sands and glass sediments. Fluid composition analyses from discrete Ti-samplers revealed Fe concentrations up to 730 μM and Alkalinity up to 21.6 meq/kg, which are the highest values found at Pele's pit. In general, the fluid composition at Mkr34 remained constant between 2006 and 2008 (Figure 4), as illustrated by the linear relationship between chemical species and Si. However, Fe/Mn ratios decreased from ~40 to 25 during that period (Figure 5). *In situ* measurements in 2006 revealed that fluids discharging from the cracks and fissures at the base of the scarp near Mkr34 reached 50°C, up from an ambient temperature of 2.6°C. Dissolved Fe^{2+} was detected by *in situ* voltammetry (648 μM) and no evidence for other aqueous iron or sulfur phases was observed (Table 3, Figure 6). In 2007 discharging fluids at vigorous venting Mkr34 orifices reached up to 53°C and Fe^{2+} of 555 μM. Mn^{2+} was also detectable *in situ* (9 μM), and evidence for low sulfide (3 μM) and aqueous FeS was detected (Table 3, Figure 6). In 2008, fluids discharging at Mkr34 had dropped to between 20°C to 51.5°C, with Fe^{2+} still enriched at 467 μM. While no free sulfide was detected, molecular clusters of FeS were detectable (Table 3).

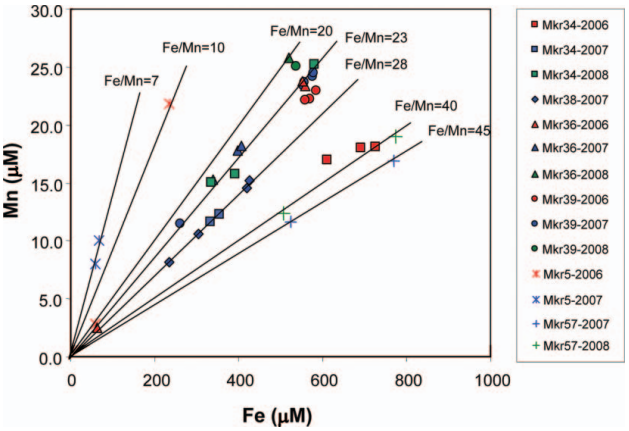

FIG. 5. Mn versus Fe for all of the discrete vent samples collected in 2006, 2007, and 2008.

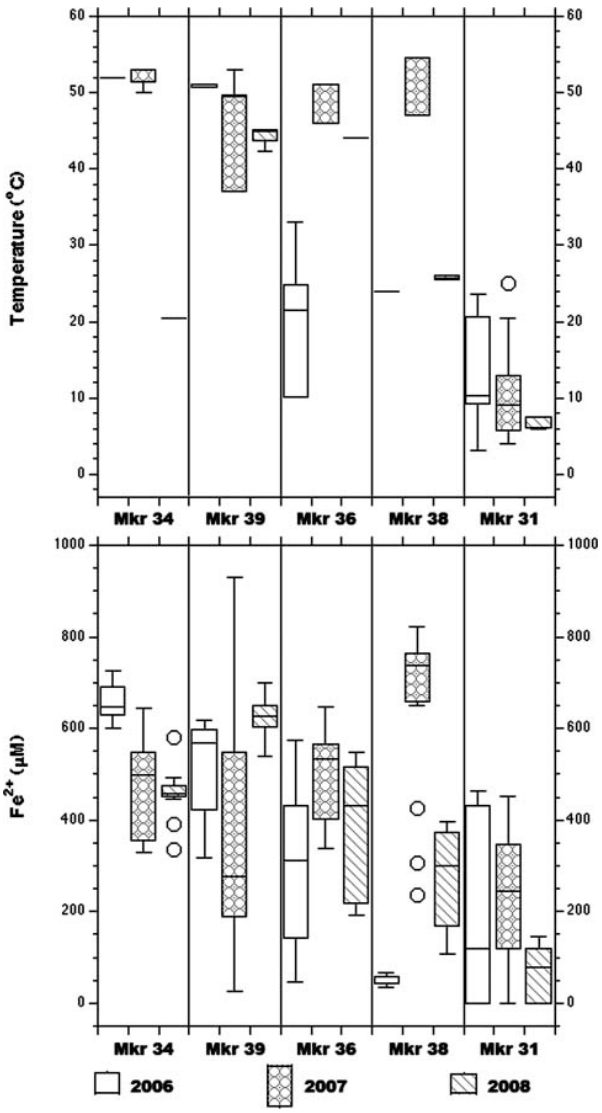

FIG. 6. Variability in temperature and Fe^{2+} for all sites of interest that were surveyed and sampled in each year using both in situ and discrete techniques. Temperature and Fe^{2+} measurements made in situ using the ROV Jason temperature wand and in situ voltammetric electrodes. Boxes represent the upper and lower quartiles, with median indicated in the box. Whiskers indicate range of data. Outliers are points whose value is greater than upper quartile + 1.5 (interquartile distance) or less than lower quartile – 1.5 (interquartile distance).

Marker 38 (18.90548440N 155.25668557W 1274.152m) is located ~20 meters away from Mkr34 along a steep scarp of the SE rim (Figure 1). Similar to Mkr34, fluids were sampled along the footwall and cracks with very little Fe-rich flocs visible in the cracks. Away from the scarp are volcanic sands and glass sediments, and microbial mats line the vertical wall. Fluid composition analyses from discrete Ti-samplers revealed Fe concentrations up to 430 μM and alkalinity up to 12.3 meq/kg. The Fe vs. Si data show that Mkr38 has very similar Fe concentrations to Mkr34, and, together with constant Fe/Mn ratios at ~ 30 between 2006 and 2007, those results suggest similar fluid sources for both vent areas, most likely affected by mixing of at least two endmembers (one with a characteristicly higher Fe/Mn ratio). Unfortunately, no fluid samples were recovered in 2008 for this site. In 2006, fluids discharging from the cracks and fissures at the base of the scarp near Mkr38 reached 51°C, up from an ambient temperature of 2.6°C. Dissolved Fe^{2+} was detected i*n situ* at 50 μM Fe^{2+} (Table 3). In 2007 fluids discharging from cracks and orifices near Mkr38 reached up to 55°C. Fe^{2+} was detected at up to 695 μM, and low level of free sulfide was detected (3 μM) (Table 3). No aqueous FeS was detected. In 2008 fluids at Mkr38 seemed to have cooled, reaching only 26°C. Dissolved Fe^{2+} was also notably lower (273 μM), but free sulfide had increased to 34 μM. Interestingly, no FeS_{aq} signal was detected.

Hiolo area (Mkr36, Mkr39, BT37, BT40)

The North Hiolo Ridge Area (Figure 1) is comprised of a ~30 m outcrop with several small cracks and orifices along the base that discharge clear shimmering fluids (Mkr36, *18.90620935N 155.25721444W 1307.628m*). Fluids were sampled along the footwall and cracks with very little Fe-rich flocs visible (Figure 2C). Away from the scarp are volcanic sands and glass sediments. In 2006, fluids discharging from the cracks and fissures at the base of the scarp near Mkr36 reached 50°C, up from an ambient temperature of 2.6°C. Dissolved iron and sulfur species in the discharging fluids included 161 μM Fe^{2+}, with traces of ~3 μM HS^- and aqueous FeS molecular clusters ($FeS_{(aq)}$). Temperature and voltammetry wand macroprofiling revealed up to 48°C and 437 μM Fe^{2+} at 4 cm below the floc-water interface, as well as the presence of aqueous FeS molecular clusters (Table 3, Figure 6). Additionally, an *in situ* microprofile was performed in flocs near Mkr36 (described in detail in section 3.2.2 below). In 2007, an actively venting orifice near Mkr36 was sampled and fluids discharging reached

50°C. Dissolved iron and sulfur species included up to 565 μM Fe^{2+}, and 23 μM HS^-, with detectable aqueous FeS molecular clusters present. In 2008, fluids discharging an active orifice near Mkr36 were observed with maximum temperature of 44°C. Fe^{2+} concentration reached 355 μM and free sulfide was detected at ~6 μM, with aqueous FeS also detectable (Table III). Fluid composition analyses from discrete Ti-samplers at Mkr36 yielded Fe and Mn concentrations of 560 and 24μM respectively, and Alkalinity up to 13 meq/kg. While Fe/Mn ratios decreased slightly from 25 to 20 between 2006 and 2008, Si-normalized Fe and Mn concentrations were higher in 2006, compared to later samplings in 2007 and 2008 as well as other vents in the area (Figure 4). Those results are best explained by significant Si precipitation, either in the subsurface or in the Ti-sampler, rather than differing fluid sources enriched in Fe and Mn.

Marker 39 (18.90629186N -155.25666221W 1301.918m) designates the Upper Hiolo Ridge Vents, which are part of the same large outcrop where Mkr36 is located (Figure 1). Several actively discharging orifices are located on the steep ridge, intersparsed with iron flocs (Figure 2D). Fluid composition analyses from discrete Ti-samplers at Mkr39 yielded Si-normalized chemical species concentrations very similar to Mkr 36, suggesting identical plumbing sources for Mkr36 and Mkr39 vents, which are located only ~10 m apart. As for Mkr36, Fe/Mn ratios decreased slightly from 25 to 21 between 2006 and 2008.

In 2006, fluids discharging from the cracks and fissures near Mkr36 reached 51°C. Dissolved iron and sulfur species included 340 μM Fe^{2+}, and consistent amounts of ~3 μM HS^- and aqueous FeS molecular clusters. Frequently, Mn(II) was also detectable *in situ* at ~20 μM. (Figure 3B, Table 3) In a finger chimney field near Mkr39 (FingChim, Table 3), similar fluid composition was observed. Temperature and voltammetry wand macroprofiling near the chimneys and surrounding flocs revealed up to 22°C and 250 μM Fe^{2+} at 17 cm below the floc-water interface, as well as the presence of aqueous Fe^{3+} clusters (Table 3). A deployed microbial sampler (BT37) was located in the surrounding Mkr39 area. No well-defined orifice was observed, but small chimneys (cm tall) are growing on thick mats. Iron flocs surrounding the sampler exhibited diffuse flow reaching up to 22°C and Fe^{2+} of 224 μM, respectively (Table 3). A similar sampler (BT40) was located nearby in fluids up to 50°C, and 569 μM Fe^{2+}. In 2007 fluids discharging from the cracks and fissures near Mkr39 reached 51°C. Dissolved iron and sulfur species included up to 312 μM Fe^{2+} at the orifice opening and up to 800 μM Fe^{2+} at 10 cm into the orifice. Consistent detectable amounts of ~50 μM free H_2S and aqueous FeS molecular clusters were also measured. At fluids emanating from the Mkr39 area, Mn(II) was frequently detectable *in situ* at ~20 μM in 2006 and 2007, but not in 2008 (Table III). In 2008, fluids discharging from the cracks and fissures at Mkr39 were up to 45°C, with Fe^{2+} concentrations at 636 μM low concentration of free sulfide (~5 μM) and detectable FeS molecular clusters (Table 3, Figure 6).

Tower area (MKr31, MKr48)

"Tower vent" north of Mkr38, 1263m; J2-241 EVT#3679: In 2006, vigorous focused discharge of shimmering fluids were detectable from cracks on the Tower outcrop, surrounded by diffuse flow through iron microbial flocs. Several individual orifices revealed temperatures in excess of 45°C, with a maximum of 52°C and 648 μM Fe^{2+}. No other dissolved iron species or sulfur species were detected in the venting fluids or within the flocs (Table 3).

Marker 31 (*18.90622331N 155.25676990W 1306.253m)* is located approximately 4 meters deeper and 30m south along the outcrop that forms the Hiolo Area. Diffuse shimmering clear fluids emanate from cracks and fissures surrounded by a patchy mixture of volcanic glass and ash sediments and iron oxide flocs. In 2006, discharging fluids surveyed in the vicinity of Mkr31 reached 9.3°C, up from an ambient temperature of 2.6 °C. No sulfur species were detected in discharging Mkr31 fluids, and all detectable Fe was present as dissolved Fe^{2+}. However, temperature and voltammetry wand macroprofiling revealed up to 24°C, 450 μM Fe^{2+}, and 3 μM HS^- at 7cm below the floc-water interface (Table 3, Figure 6). In 2007, diffuse fluids discharging from small chimneys and flocs near Mkr31 reached up to 9.5°C and 28°C at 25cm into the floc. Fe^{2+} was detected *in situ* at up to 150 μM in the discharging fluids and up to 380 μM at 25cm into the floc. Transient signals for dissolved Fe^{3+} were observed in the discharging fluids and upper centimeters of the floc (Table 3). An actively discharging orifice above Mkr31, found at 1301 m, between Mkr31 and Mkr39, was sampled and found to discharge 37°C fluids, enriched in Fe^{2+} and HS^-. In 2008 fluids emanating from small chimneys at Mkr31 reached up to 7.5°C. Fe^{2+} was 108 μM, and no other iron or sulfur species were detected (Table 3).

Marker 48 (*37 41.012N 152 47.73W, 1281m)* is located in the area between the Spillway area and Tower Area. Rocky slopes are characterized by intersparsed very thin flocs and mats with diffuse shimmering fluids. In 2007, a subsurface (−5 cm) maximum T of 11°C was found with 10 μM Fe^{2+}. Other thin areas of iron flocs revealed up to 10 μM O_2 (Table 3). Because of the very diffuse nature of low-temperature venting at Mkr31 and Mkr48, no discrete hydrothermal fluid samples have been successfully recovered.

Lohiau Area (Mkr2, Mkr5, Mkr55). Markers 2 and 5 (*18.90846700N 155.25724918W,1173.415m*) are located along the 1174 m contour of the north pit crater caldera. This area is characterized by collapsed, sedimented walls, intersparsed with rocky outcroppings. Mkr2 and Mkr5 designate two outcrops, spaced approximately 15 m from each other, and with diffuse venting cracks and fissures and iron flocs located between them. In 2006, diffuse shimmering fluids discharging through the flocs and fissures between Mkr2 and Mkr5 reached 22°C. Dissolved Fe^{2+} was detected at up to 217 μM Fe^{2+} and no evidence for other aqueous iron or sulfur phases was observed. An area of diffuse shimmering flow and iron staining just above Mkr2 and Mkr5 was much less active (<4°C). In 2007, *in situ* scans taken

directly from the diffuse flow area where 2006 exposure and colonization experiments were deployed revealed a maximum temperature of 5.5°C above the surface, and up to 19°C at 12 cm into the floc. Fluids above the surface were well-mixed with bottom waters (35 μM O_2), but reduced within the floc interior (236 μM Fe^{2+} at −10 cm). Mkr55 was deployed at an area with extensive diffuse flow and flocs in the Upper Lohiau area on J2-310 (1116 m). Diffuse flow fluids were ∼4.5°C, with a subsurface maximum of 15°C at −20 cm. In 2008, we unfortunately experienced electronic failures that compromised *in situ* electrochemical data collected in the Lohiau area.

Pohaku Area (Mkr27, Mkr57). In 2007, searches for *Marker 27* resulted in finding new areas featuring both focused flange flow and mats, although the actual Mkr27 marker was never located. Fluids = Max T ∼ 25°C, 300 μM Fe^{2+}. Insertion of the wand into the flange orifice to 30cm yielded 30°C and 934 μM Fe^{2+}, with no alternate iron or sulfur species detected (Figure 3A, Table 3). Shimmering fluids in the vicinity of Mkr57 were 18°C and 514 μM Fe^{2+}, again with no alternate iron or sulfur species detected. In 2008, a maximum temperature of 24°C was reached at 10cm into the floc, with Fe^{2+} concentration of 743 μM, and no detectable alternate iron or sulfur species.

Naha Area (Mkr1, Mkr3, Mkr6). In 2006 and 2007, *Markers 3 and 6* were found and surveyed using the temperature and *in situ* voltammetry wand. No shimmering water was visible, and localized areas that historically produced venting fluids were found to be cold (less than 2.8°C) and oxic (60 μM O_2), with no evidence for current hydrothermal discharge (Table 3).

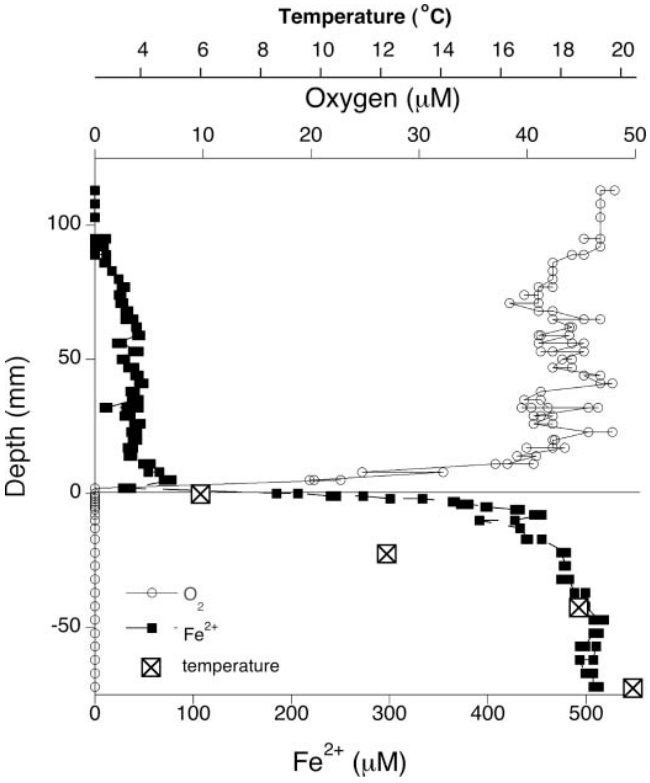

FIG. 7. In situ voltammetric microprofile collected in diffuse iron microbial flocs near Mkr 36, J2-245. Following microprofile, ROV Jason temperature wand was inserted into the floc to collect the temperature data.

Heterogeneity of Microbial Habitat at Biologically Relevant Scales

Above, we have presented a synopsis of the bulk hydrothermal fluid composition, with an overview of gross differences in temperature and chemical speciation and concentration between above-surface and below-surface habitat, as well as the range of between-site variability over a three-year sampling period. Below, we present an example of a snapshot fine-scale *in situ* characterization of the bottom-water-microbial floc interface during *in situ* voltammetric microprofiling.

In 2006, venting waters near Mkr36 were surveyed and sampled, and the MANIP (Figure 2F) was deployed in the same general area where macroprofiles had been collected (Table 3). The versatile and relatively simple tripod-manipulator package was efficiently removed from the *Jason-II* science basket and complete setup of the MANIP took approximately 25 minutes. The profile spanned from approximately 9 cm above the mat-water interface to approximately 10 cm below, with replicate voltammetric measurements collected every 1–3 mm (Figure 7). Turbulent flow and mixing of Fe^{2+} and O_2 was observed in the 1–2 cm above the mat. There was no detectable oxygen by 1mm below the mat surface, and Fe^{2+} concentrations increased steadily with depth. In voltammetry, faster scan rates can be used to offset noise induction caused by turbulent flow (Luther et al. 2002). Conversely, clean scans at slow scan rates collected from within the mat interior suggest low turbulent fluid mixing within the floc. Wand measurements were again made following profiling and temperature points were overlain on the voltammetric profile data, increasing from 6°C at the interface to 21°C in the mat interior (Figure 7). Vigorous shimmering venting waters directly adjacent to the MANIP site contained traces of sulfide as well as Fe^{2+}, but no sulfur species were detected within the mat.

DISCUSSION

Evolution of Seafloor Hydrothermal Venting at Loihi Seamount

Prior to 1996, Pele's Vents were located in the southern flank of the summit, at a water depth of 980 m (Karl et al. 1988). The active field was characterized by numerous individual vents discharging hydrothermal fluids with a maximum temperature of 31°C (Sedwick et al. 1992). In comparison with vents on MORs, hydrothermal fluid from Pele's Vents was found to be enriched in total dissolved CO_2 (up to 418 mmol/kg) and dissolved iron (up to 1460 umol/kg) and had an unusually high Fe/Mn value of ∼30 attributed to "chemical weathering" of wall rock by

magmatic volatiles entrained in the circulating hydrothermal fluids (Karl et al. 1988; Sedwick et al. 1992). In July-August 1996 a tectonic-volcanic event occurred that destroyed Pele's vents, creating a crater (Pele's pit) and several new sites of hydrothermal venting (Hilton et al. 1998; Wheat et al. 2000).

Compared to Pele's Vents, Pele's Pit vents had higher temperature (up to 200°C measured in 1997), decreased CO_2 content (Hilton et al. 1998) and decreased alkalinity and Fe/Mn values, down to 6 mol/mol at Lohiau (Wheat et al. 2000). These data were interpreted as resulting from a reduced flux of magmatic CO_2 and hence a reduced abundance of Fe in vent fluids due to diminished leaching of wallrock by carbonic acid. The occurrence of Fe- and Zn-sulfide assemblages at Lohiau also provided evidence that fluids at even higher temperatures (>250°C) and containing significant sulfide were present in the Loihi system, however, free sulfide had not been observed in venting fluids. Three years after the magmatic event, numerous diffuse low-temperature vent sites (<80°C) were reported along the south flank of Loihi (Wheat et al. 2000; Malahoff et al. 2006).

Our recent time-series of surveying and sampling (2006–2008) has revealed that in contrast to the 1996-1997 sampling, hydrothermal fluids discharging from Pele's Pit vents and southern vents at Pohaku have decreased in temperature to a range of 21.6°C to 55°C and the Naha sites have entirely ceased hydrothermal activity. The Fe/Mn ratios at Pele's Pit vents, excluding Lohiau and Pohaku, range from 20 to 40 with average of 30, similar to observations at Pele's vents before the volcanic event and three years after the collapse of the pit. This is in support of the assumption that those values likely reflect the "steady state" value for quiescent discharge at Loihi (Wheat et al. 2000; Malahoff et al. 2006).

Conversely, venting Lohiau fluids have remained relatively constant in temperature since the 1996–1997 sampling, ranging up to 25°C. Similar to 1996–1997 data, Fe/Mn ratios for Lohiau fluids are also depressed, as low as 6.8. Lower Fe/Mn ratios at Lohiau compared to higher ratios in Southern vents (>20 mol:mol, such as at Hiolo) may in part result from removal of Fe by precipitation in the subsurface. At Lohiau, two lines of evidence suggest that Fe precipitation is predominantly due to Fe-oxyhydroxide formation during fluid-seawater mixing and cooling in the subsurface: more negative overall δ^{56}Fe values than other sites (Rouxel, *unpublished*), and the absence of free sulfide or FeS_{aq} in Lohiau fluids (Table 3). While sulfide is not abundant at any vent sites at Loihi (always <50 μM), free sulfide was present in discharging fluids at the Hiolo Area (Mkr39, Mkr36, Mkr31) in each year. We also detected evidence for Fe-complexed sulfide. We interpret the FeS_{aq} signal found in select sites (e.g., Figure 3B) as the presence of iron-rich molecular clusters/nanoparticles. Such molecular clusters form as precursors to crystalline precipitation (Luther and Rickard 2005), and here support the notion that lower Fe/Mn ratios may also, in part, result from precipitation with sulfide in the subsurface (Wheat et al. 2000).

Pohaku vents (Mkr 27 and Mkr57) have historically had temperatures ranging near 20°C and high Fe/Mn ratios (23–58) (Wheat et al. 2000). During 2007–2008, we found that Pohaku had not become less active since 1996-1997, with temperatures up to 28°C and all Fe/Mn ratios >40. No free or complexed sulfide was detectable in discharging fluids (Figure 3A), suggesting an extremely iron-rich system with respect to sulfide. Wheat et al. (2000) have suggested that a longer residence time may result in more complete weathering reactions and thus a higher Fe/Mn ratio on the basis that CO_2 content, rather than water-rock ratio or chloride complexation, controls the Fe/Mn ratio in fluids at Loihi (Ding and Seyfried 1992).

Variability of Physicochemical Conditions within Fluids and Microbial Mats

Thousands of *in situ* electrochemical scans were collected with simultaneous temperature measurements and coordinated discrete samples during each cruise. Most of the Loihi Pit Crater sites were dominated by iron-rich, sulfide-deplete fluids. For electrochemistry scans collected outside of vigorous turbulent flow, and thereby intense mixing, between-scan precision was typically better than 2% (95% confidence interval). Thus, for a given sampling point within vigorous flow, between-scan variability (reported as standard deviation, Table 3, $5 < n < 10$) can largely be interpreted as real fluid mixing and composition variability, likely explaining most of the deviation from the 1:1 comparison between *in situ* measurements of Fe^{2+} and measurements of total dissolved Fe from discrete measurements (Figure 3C). Especially for sites where higher *in situ* Fe^{2+} concentrations were detected, it is likely that the *Jason* temperature wand (containing voltammetric electrodes) was spatially positioned in a microenvironment with less seawater mixing than for discrete fluid sampling. In fact, Titanium sampler snorkels were positioned centimeters away from any surfaces so as to avoid collecting floc material. In some instances where discrete sampled Fe_T concentration is significantly higher than *in situ* measured Fe^{2+}, the electrochemical data suggest significant dissolved iron species complexed with sulfide forming $FeS_{(aq)}$ in the warmest fluids (with perhaps lower subsurface residence times; e.g., Mkr39, Figure 3), or dissolved iron undergoing slow oxidation forming aqueous Fe^{3+} complexes in the cooler fluids (e.g., J2-242 diffuse finger chimney field; Druschel et al. 2008).

The variability in temperature and Fe^{2+} concentration of venting and diffuse discharging fluids over spatially integrated centimeters or time (i.e., hours to days for a given cruise) can be large for a given sampling area with some sites exhibiting much more variability in mixing between endmember fluids and seawater than others. That Loihi hydrothermal fluids support an abundant Fe-oxidizing bacterial community (e.g., Emerson and Moyer 2002) is evidence for a unique synergy between physicochemical gradients, microbial diversity within those gradients, and microbial substrate utilization, all of which can define much of the chemical speciation and biogeochemical cycling. This

synergy culminates in the extensive mats and flocs, which provide microniche stability in both temperature and hydrothermal fluid gradients. High-resolution voltammetric profiles through the flocs at Loihi reveal that the mats stabilize steep opposing gradients of O_2 and Fe^{2+} (Figure 7). Fe^{2+} advective flux through the mat and into the overlying water suggests not only that a sufficient and steady Fe^{2+} energy source is available to the microbial community in the mat, but also that the mat is potentially limited by oxidant availability. The profile also raises the intriguing possibility for community capability for iron oxidation by alternate oxidants deeper into the mats (e.g., nitrate), as O_2 is shown to rapidly decrease to undetectable concentrations ($<2\ \mu$M) just below the mat surface.

Here, we have presented the first *in situ* voltammetric microprofile for a deep-sea hydrothermal iron-oxidizing community, giving a relatively undisturbed view of gradient structure within the floc. The four common methods that have been widely used for microbial sampling at Loihi include colonization samplers, scoops, and suction sampling (Edwards, Emerson, Moyer, Tebo, Staudigel, *this issue*). Each method integrates a microbial sample over time and space, typically within the upper 10cm surrounding the floc/seawater interface, and the data presented above helps to constrain environmental conditions of microbial niches across varying spatial and temporal scales, potentially explaining some of the mat community variability (e.g., Davis and Moyer 2008).

Implications for Biomass Production

Submarine hydrothermal environments support unique biological communities based largely on the primary biomass generated *in situ* by chemolithoautotrophic microorganisms that catalyze energetically favorable redox reactions for energy gain and metabolic growth (Jannasch et al. 1995; Karl et al. 1995). Several groups of prokaryotes are known to catalyze ferrous iron oxidation using O_2 (Emerson and Moyer 1997; Sobolev and Roden 2001; Edwards et al. 2003, 2004; Roden et al. 2004):

$$4Fe^{2+} + O_{2(aq)} + 4H^+ \rightarrow 4Fe^{3+} + 2H_2O \qquad [1]$$

At a pH much above 4.0, the ferric iron rapidly precipitates, mainly as ferrihydrite:

$$Fe^{3+} + 3H_2O \rightarrow Fe(OH)_3 + 3H^+ \qquad [2]$$

or a combined reaction of:

$$Fe^{2+} + 1/4O_{2(aq)} + 2\ 1/2H_2O = Fe(OH)_{3(s)} + 2H^+ \qquad [3]$$

Abiotic chemical oxidation of ferrous iron also proceeds spontaneously; Fe(II) oxidation rates in hydrothermal plumes have been estimated with Fe(II) half-life (t) varying from a few minutes for some Atlantic sites with $O_2 \sim 250$ uM to hours at Pacific sites with $O_2 \sim 100$ uM (Rudnicki and Elderfield 1993; Field and Sherrell 2000; Statham et al. 2005).

The extreme Fe^{2+} and O_2 gradients encountered within microbial mats at Loihi are likely supporting the vast majority of biomass production in this environment. In addition to high-temperature venting, it is most likely that the energy source supporting this microbial community is Fe^{2+} that is advected into the mat from Fe-rich fluids from below. Bioenergetic calculations based on chemolithoautotrophic growth yields for cells sustaining growth on Fe^{2+} can provide estimates of the potential energy that is available for biomass production (Heijnen and van Dijken 1992; McCollom 2000). For example, Edwards et al. (2004) calculated, based on an estimated Fe flux derived from an estimated overall heat budget for Loihi and measured fluid chemistries, that the Gibbs energy for Fe oxidation at Loihi could support approximately 20 kg of biomass C per day. Based upon the high-resolution *in situ* profile for O_2 and Fe^{2+}, we can attempt to re-evaluate and constrain this estimation for Loihi microbial mat habitats. For example, the reaction energetics for Equation 1 can be calculated according to the equation:

$$\Delta G_R = \Delta G^0 + RT \ln Q \qquad [4]$$

where ΔG_R and ΔG^0 are the Gibbs energy and the standard Gibbs energy of the reaction, R is the molar gas constant, T is the temperature in Kelvin, and Q is the activity quotient of the reactants and products. We assume diffusivity for $O_{2(aq)}$ to be 10^{-5} cm^2 s^{-1}, over a 5 cm depth across the mat-water interface. We use the extended Debye-Huckel equation with an ionic strength of 0.7 M to estimate an activity coefficient for Fe^{2+} of 0.23. We also assume 90% of the Fe^{2+} within the mat interior to be free (excluding organic complexes), yielding an Fe^{2+} activity of 105 μM. At an estimated $O_{2(aq)}$ activity of 1 μM near the mat surface, the Gibbs energy of reaction is -298 kJ/mol O_2 for the complete reaction (Equation 3). And even at very low O_2 activities (1 nM and 1 pM) the reaction is still strongly exergonic (-281 kJ/mol O_2 and -264 kJ/mol O_2, respectively). The *in situ* profiles reveal that O_2, not Fe^{2+} is the limiting reactant, and therefore Fe oxidation should be controlled by the rate of diffusion of O_2 into the mat (and/or alternate less energetically favorable oxidants such as nitrate are potentially being utilized). The decrease of O_2, from 45 μM above the mat to $<2\ \mu$M at the mat surface, indicates a diffusive flux of at least 2×10^{-6} moles cm^{-2} a^{-1}. This O_2 flux equates to an energy flux of $\sim$0.6 J cm^{-2} a^{-1}. Assuming that aerobic autotrophs require 292 kJ to fix 1g of C (Heijnen and van Dijken 1992), and the average cell contains between 5×10^{-15} g C and 20×10^{-15} g C (Whitman 1998), an energy flux of 0.6 J cm^{-2} a^{-1} could support the growth of 1×10^7 to 4×10^8 cells cm^{-2} a^{-1}.

Implications for Hydrothermal Fe Fluxes

It has long been established that hydrothermal plumes modify the gross flux of many chemicals from vent-fluids to the

oceans and remove other dissolved tracers from the overlying water column (e.g., German and Von Damm 2004). However, the possible far-field consequences of hydrothermally-released Fe, in comparison to sources such as riverine, aerial, and sediment inputs to global ocean, is unknown. This question is particularly important because Fe is widely recognized as a limiting nutrient in large regions of world's ocean (Martin 1990; Hutchins et al. 1999; Archer and Johnson 2000; Boyd et al. 2000). Although most Fe is readily precipitated in hydrothermal plumes, in the form of Fe-oxides and/or Fe-sulfides, it has been recently reported that the formation of Fe-ligand complexes in the hydrothermal environment can both stabilize Fe(III) in solution and decrease the rate of Fe(II) oxidation (Bennett et al., 2008; Toner et al., 2009). Especially understudied is the relative input from off-axis hydrothermal sources, such as seamounts.

Using previous estimates of Fe(II) oxidation rates in hydrothermal plumes, we can determine an Fe(II) half-life (t) of about 12 hours above Pele's pit ($O_2 \sim 50\ \mu M$) which is more than twice higher than for most hydrothermal plume above East Pacific Rise (Field and Sherrell 2000; Statham et al. 2005). Hence, in addition to potential C-complexation and stabilization of Fe in hydrothermal plume, the slow rate of Fe(II) oxidation may contribute to far-field Fe influences. In particular, microbial processes in the hydrothermal plume at Loihi likely play an important role in controlling Fe oxidation kinetics, chemical speciation, mineralogy, and Fe stabilization.

CONCLUSION

Seafloor hydrothermal activity is one of the fundamental processes controlling the exchange of heat and chemical species between seawater and ocean rocks (Edmond et al. 1979; Stein and Stein 1995; Elderfield and Schultz 1996; Wheat et al. 2004). The abundance of Fe in high-temperature hydrothermal fluids at mid-ocean ridges and hydrothermally-active seamounts, along with its oxidation-reduction properties, confers it a particularly important role in both the chemistry and biology of near-field seafloor hydrothermal environments (Edwards et al. 2003). Certain environmental niches exist today, and have possibly been plentiful in Earth's history however, where the kinetics of abiotic oxidation are more sluggish, and biologically favorable conditions prevail, allowing microbes to be competitive with abiotic reactions. Our work at Loihi identifies a diversity of habitats ranging from iron-rich venting hydrothermal fluids to microbially mediated Fe^{2+} - O_2 gradients where FeOB are plentiful, and further illustrates the usefulness of the application of *in situ* voltammetric methods to complement traditional discrete sampling and geochemical analyses. Specifically, *in situ* voltammetry has been quite useful during real-time surveying and identification of microbial niches and redox gradients, thus validating sampling and deployment locations.

REFERENCES

Archer DE, Johnson K. 2000. A model of the iron cycle in the ocean. Global Biogeochem Cycles 14:269–279.

Bennett SA, Achterberg EP, Connelly DP, Statham PJ, Fones GR, German CR. 2008. The distribution and stabilization of dissolved Fe in deep-sea hydrothermal plumes. Earth Planet Sci Lett 270:157–167.

Boyd PW, Watson AJ, Law CS, Abraham ER, Trull T, Murdoch T, Bakker DCE, Bowie A, Buesseler KO, Chang H, Charette M, Croot P, Downing K, Frew R, Gall M, Hadfield M, Hall J, Harvey M, Jameson G, DeLaRoche J, Liddicoat M, Ling R, Maldonado MT, McKay RM, Nodder S, Pickmere S, Pridmore R, Rintoul S, Safi K, Sutton P, Strzepek R, Tanneberger K, Turner S, Waite A, Zeldis J. 2000. A mesoscale phytoplankton bloom in the polar Southern Ocean stimulated by iron fertilization. Nature 407:695–702.

Brendel PJ, Luther GW. 1995. Development of a gold amalgam voltammetric microelectrode for the determination of dissolved Fe, Mn, O_2, and S(-II) in porewaters of marine and freshwater sediments. Environ Sci Technol 29(3):751–761.

Bristow G, Taillefert M. 2008. VOLTINT: A Matlab-based program for semi-automated processing of geochemical data acquired by voltammetry. Comput Geosci 34(2):153–162.

Davis RE, Moyer CL. 2008. Extreme spatial and temporal variability of hydrothermal microbial mat communities along the Mariana Island Arc and southern Mariana back-arc system. J Geophys Res 113(B8): B08S15. doi: 10.1029/2007JB005413.

Ding K, Seyfried JWE. 1992. Determination of Fe-Cl complexing in the low pressure supercritical region (NaCl fluid): Iron solubility constraints on pH of subseafloor hydrothermal fluids. Geochim Cosmochim Acta 56:3681–3682.

Druschel GK, Emerson D, Sutka R, Suchecki P, Luther GW. 2008. Low-oxygen and chemical kinetic constraints on the geochemical niche of neutrophilic iron(II) oxidizing microorganisms. Geochim Cosmochim Acta 72:3358–3370.

Edmond JM, Measures C, McDuff RE, Chan, LH, Collier R, Grant B, Gordon LI, Corliss JB. 1979. Ridge crest hydrothermal activity and the balances of the major and minor elements in the ocean: The Galapagos data. Earth Planet Sci Lett 46:1–18.

Edwards KJ, Bach W, McCollom TM. 2004. Neutrophilic iron-oxidizing bacteria in the ocean: their habitats, diversity, and roles in mineral deposition, rock alteration, and biomass production in the deep-sea. Geomicrobiol J 21:393–404.

Edwards KJ, Bach W, Rogers DR. 2003. Geomicrobiology of the ocean crust: a role for chemoautotrophic Fe-bacteria. Biol Bull 204:180–185.

Elderfield H, Schultz, A. 1996. Mid-ocean ridge hydrothermal fluxes and the chemical composition of the ocean. Ann Rev Earth Planet Sci 24:191–224.

Emerson D. Potential for iron-reduction and iron-cycling in iron oxyhydroxide-rich microbial mats at Loihi Seamount. Geomicrobiol J, in press.

Emerson D, Moyer CL. 1997. Isolation and characterization of novel iron-oxidizing bacteria that grow at circumneutral pH. Appl Environ Microbiol 63(12):4784–4792.

Emerson D, Moyer CL. 2002. Neutrophilic Fe-oxidizing bacteria are abundant at the Loihi seamount hydrothermal vents and play a major role in Fe oxide deposition. Appl Environ Microbiol 68:3085–3093.

Field MP, Sherrell, RM. 2000. Dissolved and particulate Fe in a hydrothermal plume at 9 degrees 45' N, East Pacific Rise: slow oxidation kinetics in Pacific plumes. Geochim Cosmochim Acta 64(4):619–628.

Garcia MO, Caplan-Auerbach J, DeCarlo EH, Kurz MD, Becker N. 2006. Geology, geochemistry and earthquake history of Loihi Seamount, Hawaii's youngest volcano. Chemie der Erde Geochem 66(2):81.

German CR, Von Damm KL. 2004. Hydrothermal Processes. In: Holland HD, Turekian KK, editors. Treatise on Geochemistry Volume 6: The Oceans and Marine Geochemistry. Chapter 6.07. Elsevier, Oxford, UK P 181–222.

Glazer BT, Luther GW, Konovalov SK, Friederich GE, Nuzzio DB, Trouwborst RE, Tebo BM, Clement BG, Murray K, Romanov AS. 2006a.

Documenting the suboxic zone of the Black Sea via high-resolution real-time redox profiling. Deep Sea Res Pt II: Top Stud Oceanogr 53(17–19):1740–1755.

Glazer BT, Luther GW, Konovalov SK, Friederich GE, Trouwborst RE, Romanov AS. 2006b. Spatial and temporal variability of the Black Sea suboxic zone. Deep Sea Res Pt II: Top Stud Oceanogr 53(17–19):1756–768.

Glazer BT, Marsh AM, Stierhoff K, Luther GW. 2004. The dynamic response of optical oxygen sensors and voltammetric electrodes to temporal changes in dissolved oxygen concentrations. Anal Chim Acta 518:93–100.

Glazer BT, Cary SC, Hohmann L, Luther GW. 2002. In situ sulfur speciation using Au/Hg microelectrodes as an aid to microbial characterization of an intertidal salt marsh microbial mat. In: Taillefert M, Rozan TF, editors. Environmental Electrochemistry: Analyses of Trace Element Biogeochemistry. New York: American Chemical Society. P283–304.

Heijnen JJ, Van Dijken JP. 1992. In search of a thermodynamic description of biomass yields for the chemotrophic growth of microorganisms. Biotechnol Bioeng 39:833–858.

Hilton DR, McMurtry GM, Goff F. 1998. Large variations in vent fluid $CO_2/^3He$ ratios signal rapid changes in magma chemistry at Loihi Seamount, Hawaii. Nature 396:359–362.

Hsu-Kim H, Mullaugh KM, Tsang JJ, Yucel M, Luther GW. 2008. Formation of Zn- and Fe-sulfides near hydrothermal vents at the Eastern Lau spreading center: implications for sulfide bioavailability to chemoautotrophs. Geochem Trans 9(6). doi:10.1186/1467-4866-9-6.

Hutchins DA, Witter AE, Butler A, Luther GW. 1999. Competition among marine phytoplankton for different chelated iron species. Nature 400:858–861.

Jannasch HW. 1995. Microbial interactions with hydrothermal fluids. In: Humphris SE, Zierenberg R A, Mullineaux LS, Thomson RE, editors. Seafloor hydrothermal Systems: Physical, Chemical, Biological, and Geological Interactions. American Geophysical Union. Washington, DC, USA P273–296.

Karl DM. 1995. Ecology of free-living hydrothermal vent microbial communities. In: Karl DM, editor. Microbiology of extreme and unusual environments. Deep-sea hydrothermal vent habitats. New York, CRC Press. P35–124.

Karl DM, McMurtry, GM. 1988. Loihi Seamount, Hawaii: a mid-plate volcano with a distinctive hydrothermal system. Nature 335:532–535.

Konovalov SK, Luther GW, Friederich GE, Nuzzio DB, Tebo BM, Murray JW, Oguz T, Glazer BT, Trouwborst RE, Clement BG, Murray KJ, Romanov AS. 2003. Lateral injection of oxygen with the Bosporus plume-fingers of oxidizing potential in the Black Sea. Limnol Oceanogr 48(6):2369–2376.

Lewis B, Glazer BT, Montbriand PJ, Luther GW, Nuzzio DB, Ma S, Theberge SM. 2007. Short-term and interannual variability of redox-sensitive chemical parameters in hypoxic/anoxic bottom waters of the Chesapeake Bay. Mar Chem 105:296–308.

Lovely DR. 1991. Dissimilatory Fe(III) and Mn(IV) reduction. Microbiol Rev 55:259–287.

Luther GW, Bono AB, Taillefert M. 2002. A continuous flow electrochemical cell for analysis of chemical species and ions at high pressure: laboratory, shipboard and hydrothermal vent results. In: Taillefert M, Rozan TF, editors. Environmental Electrochemistry: Analyses of Trace Element Biogeochemistry. Washington, DC: American Chemical Society. P54–73.

Luther GW, Brendel PJ, Lewis BL, Sundby B, Lefrancois L, Silverberg N, Nuzzio DB. 1998. Simultaneous measurement of O_2, Mn, Fe, I^-, and S(-II) in marine pore waters with a solid-state voltammetric microelectrode. Limnol Oceanogr 43(2):325–333.

Luther GW, Glazer BT, Hohmann L, Popp J, Taillefert M, Rozan TF, Brendel PJ, Theberge SM, Nuzzio DB. 2001. Sulfur speciation monitored *in situ* with solid state gold amalgam voltammetric microelectrodes: polysulfides as a special case in sediments, microbial mats and hydrothermal vent waters. J Environ Monitor 3(1):61–66.

Luther GW, Glazer BT, Ma S, Trouwborst RE, Moore TS, Metzger E, Kraiya C, Waite T, Druschel G, Sundby B, Taillefert M, Nuzzio DB, Shank TM, Lewis BL, Brendel PJ. 2008. Use of voltammetric solid-state (micro)electrodes for studying biogeochemical processes: from laboratory measurements to real time measurements with an *in situ* electrochemical analyzer (ISEA). Mar Chem 108:221–235.

Luther GW, Reimers CE, Nuzzio DB, Lovalvo D. 1999. In situ deployment of voltammetric, potentiometric, and amperometric microelectrodes from a ROV to determine dissolved O_2, Mn, Fe, S(-2), and pH in porewaters. Sea Technol 33(23):4352–4356.

Luther GW, Rickard DT. 2005. Metal sulfide cluster complexes and their biogeochemical importance in the environment. J Nanopart Res **7**(6):713–733.

Luther GW, Rozan TF, Taillefert M, Nuzzio DB, DiMeo C, Shank TM, Lutz RA, Cary SC. 2001. Chemical speciation drives hydrothermal vent ecology. Nature 410(6830):813–816.

Malahoff A. 1987. Geology of the summit of Loihi submarine volcano. In: Decker RW, Wright TL, Stauffer PH, editors. Volcanism in Hawaii: U.S. Geological Survey Professional Paper 1350: 133–144.

Malahoff A, Kolotyrkina IY, Midson BP, Massoth GJ. 2006. A decade of exploring a submarine intraplate volcano: hydrothermal manganese and iron at Loihi volcano, Hawaii. Geochem Geophys Geosyst 7:Q06002. doi:10.1029/2005GC001222.

Martin JH. 1990. Glacial-interglacial CO_2 change: the iron hypothesis. Paleoceanography 5:1–13.

McCollom TM. 2000. Geochemical constraints on primary productivity in submarine hydrothermal vent plumes. Deep Sea Research Part I: Oceanogr Res Papers 47(1):85–101.

Moyer CL, Dobbs FC, Karl DM. 1994. Estimation of diversity and community structure through restriction fragment length polymorphism distribution analysis of bacterial 16S rRNA genes from a microbial mat at an active hydrothermal vent system, Loihi Seamount, Hawaii. Appl Environ Microbiol 60:871–879.

Moyer CL, Dobbs FC, Karl DM. 1995. Phylogenetic diversity of the bacterial community from a microbial mat at an active, hydrothermal vent system, Loihi Seamount, Hawaii. Appl Environ Microbiol 61(4):1555–1562.

Moyer CL, Tiedje JM, Dobbs FC, Karl DM. 1998. Diversity of deep-sea hydrothermal vent Archaea from Loihi Seamount, Hawaii. Deep Sea Res II 45:303–317.

Roden EE, Sobolev D, Glazer BT, Luther GW. 2004. Potential for microscale bacterial Fe redox cycling at the aerobic-anaerobic interface. Geomicrobiol J 21:379–391.

Rudnicki MD, Elderfield H. 1993. A chemical model of the buoyant and neutrally buoyant plume above TAG vent filed, 26 degree north, Mid-Atlantic Ridge. Geochim Cosmochim Acta 87:2939–2957.

Sedwick PN, McMurtry GM, Macdougall JD. 1992. Chemistry of hydrothermal solutions from Pele's Vents, Loihi Seamount, Hawaiï. Geochim Cosmochim Acta 56:3643–3667.

Sobolev D, Roden EE. 2001. Suboxic deposition of ferric iron by bacteria in opposing gradients of Fe(II) and oxygen at circumneutral pH. Appl Environ Microbiol 67(3):1328–1334.

Statham PJ, German CR, Connelly DP. 2005. Iron (II) distribution and oxidation kinetics in hydrothermal plumes at the Kairei and Edmond vent sites, Indian Ocean. Earth Planet Sci Lett 236(3/4):588–596.

Stein CA, Stein S, Pelayo A. 1995. Heat flow and hydrothermal circulation. In: Humphriris SE, Ziernberg RA, Mullineaux LS, Thomson RE, editors. Seafloor hydrothermal systems: physical, chemical, biological, and geological interactions. AGU Monograph No. Washington, DC, USA 91:425–445.

Taillefert MT, Neuhuber S, Bristown G. 2007. The effect of tidal forcing on biogeochemical processes in intertidal salt marsh sediments. Geochem Trans 8:6. doi:10.1186/1467-4866-8-6.

Toner BM, Fakra SC, Manganini SJ, Santelli CM, Marcus MA, Moffett JW, Rouxel O, German CR, Edwards KJ. 2009. Preservation of iron(II) by carbon-rich matrices in a hydrothermal plume. Nat Geosci doi:10.1038/ngeo433.

Von Damm KL, Edmond JM, Grant B, Measures CI, Walden B, Weiss RF. 1985. Chemistry of submarine hydrothermal solutions at 21°N, East Pacific Rise. Geochim Cosmochim Acta 49:2197–2220.

Wheat CG, Jannasch HW, Plant JN, Moyer CL, Sansone FJ, McMurtry GM. 2000. Continuous sampling of hydrothermal fluids from Loihi Seamount after the 1996 event. J Geophys Res 105:19353–19367.

Wheat CG, Mottl MJ, Fisher AT, Kadko D, Davis EE, Baker E. 2004. Heat flow through a basaltic outcrop on a sedimented young ridge flank. Geochem Geophys Geosyst 5(12):1–18.

Whitman WB, Coleman DC, Wiebe WJ. 1998. Prokaryotes: The unseen majority. Proc Natl Acad Sci USA 95:6578–6583.